

Research Article

Structural and Morphological Characterization of Micro and Nanofibers Produced by Electrospinning and Solution Blow Spinning: A Comparative Study

Juliano E. Oliveira,^{1,2} Luiz H. C. Mattoso,² William J. Orts,³ and Eliton S. Medeiros⁴

¹ Departamento de Engenharia de Materiais (DEMA), Universidade Federal de São Carlos (UFSCAR), Rodovia Washington Luis, KM 235, Monjolinho, 13.565-905 São Carlos, SP, Brazil

² Laboratório Nacional de Nanotecnologia para o Agronegócio (LNNA), Embrapa Instrumentação Agropecuária (CNPDIA), Rua XV de Novembro, 1452 Centro, 13.560-970 São Carlos, SP, Brazil

³ United States Department of Agriculture (USDA), Western Regional Research Center (WRRRC), Bioproduct Chemistry and Engineering (BCE), 800 Buchanan Street, Albany, CA 94710, USA

⁴ Universidade Federal da Paraíba (UFPB), Departamento de Engenharia de Materiais (DEMAT), Cidade Universitária, 58.051-900 João Pessoa, PB, Brazil

Correspondence should be addressed to Eliton S. Medeiros; eliton_s@yahoo.com

Received 24 February 2013; Accepted 8 April 2013

Academic Editor: Pavel Lejcek

Copyright © 2013 Juliano E. Oliveira et al. This is an open access article distributed under the Creative Commons Attribution License, which permits unrestricted use, distribution, and reproduction in any medium, provided the original work is properly cited.

Nonwoven mats of poly(lactic acid) (PLA), poly(ethylene oxide) (PEO), and poly(ϵ -caprolactone) (PCL) were prepared at a nano- and submicron scale by solution blow spinning (SBS) and electrospinning in order to compare crystalline structure and morphology developed by both processes during fiber formation. Polymer solutions were characterized by rheometry and tensiometry. Spun fibers were characterized by several analytical steps. SEM analyses showed that both solution blow spun and electrospun fibers had similar morphology. Absence of residual solvents and characteristic infrared bands in the solution blow spun fibers for PLA, PCL, and PEO was confirmed by FTIR studies. XRD diffraction patterns for solution blow spun and electrospun mats revealed some differences related to distinct mechanisms of fiber formation developed by each process. Significant differences in thermal behavior by DSC were observed between cast films of PLA, PCL, and PEO and their corresponding spun nanofibers. Furthermore, the average contact angles for spun PLA and PCL were higher than for electrospun mats, whereas it was slightly lower for PEO. When comparing electrospun and solution blow spun fibers, it was possible to verify that fiber morphology and physical properties depended both on the spinning technique and type of polymer.

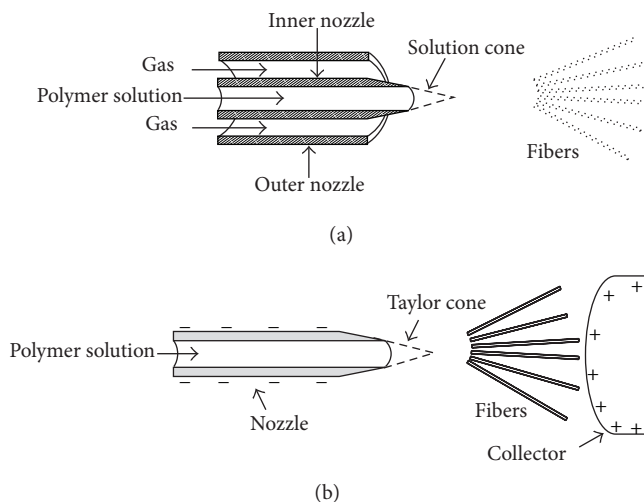
1. Introduction

Polymer fibers are used in a wide variety of applications ranging from scaffolding biomaterials, textiles, and sensors to composite reinforcement and filtration [1]. Traditional methods used to obtain polymer fibers include melt spinning [2–4], solution spinning, and gel-state fiber forming [5]. These methods can be used to produce fibers with diameters of a few nanometers; however, in most cases, fiber diameter lies in the micron scale [6].

Since the 1990s there has been an increasing interest in methods of fiber production such as electrospinning [7–9],

which can consistently produce submicron and nanometric fibers from a variety of polymers, including PLA, PCL, and PEO [1, 10–12]. The preparation of nanofibers from these polymers for tissue engineering applications was recently reported in the literature [13].

Recently, another method of fiber production, known as solution blow spinning (SBS), was developed that is conceptually similar to electrospinning without the voltage requirement and also retains elements of solution spinning. This method has been successfully used to produce micro- and nanofibers of polymers with diameters ranging from a few tenths of nanometers to several microns, depending



SCHEME 1: Cutaway diagram of the (a) concentric nozzle system used in solution blow spinning and (b) electrospinning processes.

on the experimental conditions used [14–17]. This technique applies a novel pair of concentric nozzles in which a polymer solution is forced through the inner nozzle at an appropriate rate. The droplet formed at the tip of the inner nozzle is then stretched by a high-pressure stream of compressed gas flowing around the droplet through the outer nozzle (Scheme 1(a)). This causes the surface of the drop to distort into a conical shape (solution cone) somewhat similar to electrospinning (Scheme 1(b)). When a critical air pressure is exceeded, this solution jets from the apex of the cone towards its target. As these jets travel across the working distance, they are stretched by the pressure drop, while the solvent evaporates, leaving behind polymer fibers which can be collected, basically, on any target. By varying polymer architecture and processing conditions, polymer fibers can be spun with a large surface area for different potential applications such as membranes for biological and chemical sensors, drug delivery, filtration media, and tissue engineering [14, 16, 18].

The goal of this work was to study, by solution blow spinning and electrospinning, different polymer/solvent systems from which micro- and nanofibers are produced. Crystalline and amorphous polymers, including poly(ethylene oxide) (PEO), poly(lactid acid) (PLA), and poly(ϵ -caprolactone) (PCL), were spun from different solvent systems to investigate the influence of polymer type and processing parameters on fiber structure and morphology. Spun samples were characterized by scanning electron microscopy (SEM), X-ray diffraction (XRD), thermogravimetry (TG), differential scanning calorimetry (DSC), and contact angle measurements. Fourier-transform infrared spectroscopy (FTIR) was also used in order to verify the presence of residual solvent on the spun fibers.

2. Experimental

2.1. Preparation and Characterization of Polymer Solutions. Poly(lactic acid), PLA, ($M_n = 75,000 \text{ g}\cdot\text{mol}^{-1}$) was obtained

TABLE 1: Solution parameters of spun fibers.

Polymer	Concentration (wt. %)	Solvent (v/v)
PLA	6	Chloroform : acetone 3 : 1
PCL	6	Dichloromethane
PEO	6	Dichloromethane

from Biomater (São Carlos, Brazil). Poly(ϵ -caprolactone), PCL, ($M_n = 50,000 \text{ g}\cdot\text{mol}^{-1}$) was obtained from Perstorp (Warrington, UK), and poly(ethylene oxide), PEO, ($M_n = 100,000 \text{ g}\cdot\text{mol}^{-1}$) was obtained from Sigma-Aldrich (USA). Chemical structures of these polymers are shown in Figure 1. Chloroform, dichloromethane, and acetone, purchased from Synth (São Paulo, Brazil), were used to prepare the polymer solutions used in this study. In order to prepare these solutions for solution blow spinning and electrospinning, weighed amounts of PLA, PCL, and PEO were dissolved according to proportions listed in Table 1 and under vigorous stirring for several hours until complete dissolution.

2.2. Characterization of the Solutions. Solution properties, such as surface tension (γ) and shear viscosity (η), were measured at ambient temperature using a Kibron Microtrough X pressure sensor and an Anton Paar Physica MCR rheometer, respectively.

2.3. Fiber Spinning. Fibers prepared by electrospinning were spun using a voltage of 24 kV, working distance of 12 cm, and a feed rate of $2 \mu\text{L}\cdot\text{min}^{-1}$. Fibers obtained by solution blow spinning were prepared under an air pressure of 0.4 MPa, working distance of 12 cm, and feed rate of $120 \mu\text{L}\cdot\text{min}^{-1}$. In both cases, a polymer concentration of 6 wt.% was used.

2.4. Fiber Characterization

2.4.1. SEM. Fiber morphology was observed using a model DSM960 Zeiss scanning electron microscope (SEM), after gold coating with a sputter coater (Balzers, SCD 050). Fiber diameters were measured with the aid of image software (ImageJ, National Institutes of Health, USA). For each experiment, average fiber diameter and distribution were determined from about 100 random measurements using micrographs representative of fiber morphology.

2.4.2. FTIR. FTIR data were recorded on a Nicolet 470 Nexus FTIR spectrometer. The FTIR spectrometer was purged continuously with nitrogen. A total of 64 scans were collected with a resolution of 2 cm^{-1} . The infrared spectra were recorded in transmission mode using thick films of spun (solution blow spinning and electrospinning) polymer nanofibers which were deposited on a silicon wafer.

2.4.3. XRD Characterization. For XRD measurements, non-woven fibrous mats, which were collected on aluminum foils, were deposited on circular glass slides for further analyses. X-ray diffraction patterns were recorded using a Shimadzu

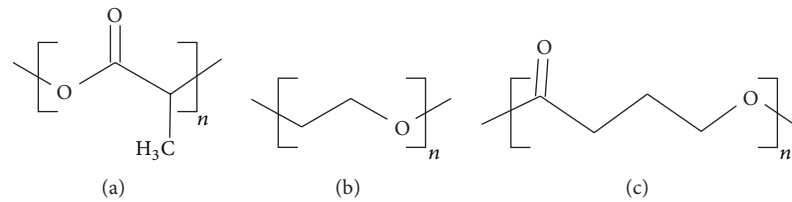


FIGURE 1: Chemical structure of the polymers used for fiber spinning: (a) PLA, (b) PEO and (c) PCL.

XRD-6000 diffractometer. Scans were carried out from 10° to 30° (2θ) at a scan rate of $2^\circ/\text{min}$ using Ni-filtered $\text{CuK}\alpha$ radiation. The full width at half-maximum height (FWHM) of the diffraction peaks was calculated by fitting the X-ray diffraction data with a Gaussian-Lorentzian function (Origin 7.5 software, Origin Lab, USA). The d -spacing for a given scattering angle, 2θ , was calculated by application of the Bragg equation

$$d = \frac{\lambda}{2 \sin \theta}, \quad (1)$$

where λ is the wavelength of the $\text{CuK}\alpha$ radiation ($\lambda = 0.154 \text{ nm}$).

The full width at half-maximum height of the diffraction peaks was calculated by fitting the X-ray diffraction data with a Lorentzian function, and the crystallite size, D , was estimated by calculating the broadening of the diffraction peaks according to the Scherrer equation

$$D = \frac{k\lambda}{\beta \cos \theta}, \quad (2)$$

where k is the Scherrer constant that depends upon lattice direction and crystallite morphology, and β is the full width at half-maximum height given in radians. A k value of 0.9 was used in this study, which is based on values found in the literature for these polymers [19–22].

2.4.4. Thermal Analyses. TG experiments were performed on a Q500 TA Instruments thermogravimetric analyzer under nitrogen atmosphere, at a flow rate of $20 \text{ ml}\cdot\text{min}^{-1}$. Samples were scanned from room temperature to 600°C at a scanning rate of $10^\circ\text{C}/\text{min}$ using platinum crucibles.

DSC studies were performed on a Q100 TA Instruments calorimetric analyzer under nitrogen atmosphere, at a flow rate of $20 \text{ mL}/\text{min}$. The samples were heated from 10°C to 200°C for PLA, -70°C to 110°C for PCL, and -20°C to 120°C for PEO at a scanning rate of $10^\circ\text{C}/\text{min}$ using aluminum pans.

2.4.5. Contact Angle Measurements. Contact angles of water on the surface of spun fibers (nonwoven mats) were measured by a CAM 101 model KSV Instruments equipped with a CCD camera (KGV-5000). In each measurement, a $5 \mu\text{L}$ droplet was pipetted onto the surface, and images of the droplet were automatically taken as a function of time. From these images, contact angle values were calculated using dedicated software (KSV CAM2008). Measurements were carried out at 25°C and about 53% humidity.

TABLE 2: Experimental values of surface tension in mN/m for the polymer solutions and solvents (23°C , 43% RH).

Polymer solution (6% wt)	γ (mN/m)	Solvent	γ (mN/m)
PLA	50.0	Chloroform	27.8
PEO	42.9	Dichloromethane	28.6
PCL	51.0	Acetone	25.6
		Chloroform : acetone 3 : 1 (v/v)	26.7

3. Results and Discussion

3.1. Solution Characterization. Values of viscosity (10^{-1} s^{-1}) for PLA, PEO, and PCL were found to be, respectively, 13, 71, and $35 \text{ mPa}\cdot\text{s}$. These differences can be attributed to polymer structures and molecular weights as well as polymer-solvent interactions. According to the manufacturers, these polymers have a number-average molecular weight (\bar{M}_n), respectively, of 75,000, 100,000, and $50,000 \text{ g}\cdot\text{mol}^{-1}$ which can account for the differences in the viscosity values found. Although the molecular weight of PCL is lower than that of PLA, its higher value of viscosity can be attributed to the polar ester groups in PCL that promote stronger interchain interactions. Moreover, other factors that play an important role in polymer chain configuration [23], and therefore, in viscosity, such as polymer-solvent interaction parameters, may also be contributing to these differences found.

Solutions showed similar values of surface tension ($34, 37, \text{ and } 39 \text{ mN}\cdot\text{m}^{-1}$, respectively, to PLA, PEO, and PCL), which can be due to the low concentration of polymer (6 wt.%) as well as because of differences in surface tension of each polymer and solvent, as can be seen in Table 2.

The knowledge of solution properties such as viscosity and surface tension is important to understand fiber morphology. Viscoelasticity was found to be one of the parameters that most influenced the morphology of solution blow spun fibers [14, 24]. On the other hand, surface tension is known to play a major role in fiber morphology developed during the electrospinning process [25].

3.2. Morphological Characterization. SEM micrographs of PLA, PEO, and PCL fibers are shown in Figures 1(a)–1(c). Fiber average diameters, calculated using about 100 individual diameters to each sample, are shown in Table 3.

As outlined by the data trends in Table 3 and the micrographs (Figure 2), fiber morphology was different in each

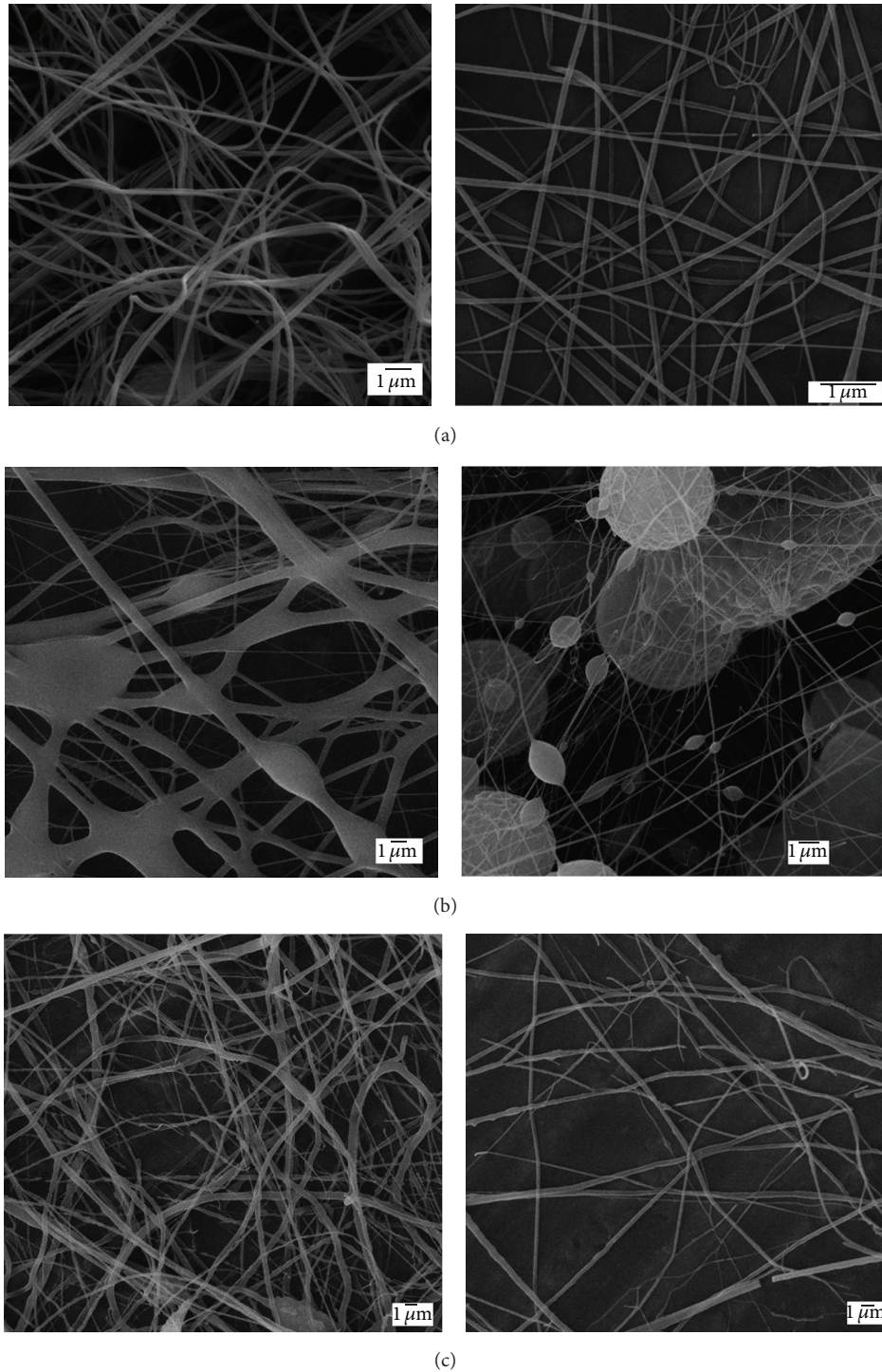


FIGURE 2: Scanning electron micrographs of spun fibers obtained by solution blow spinning and electrospinning for PLA (a), PCL (b), and PEO (c). Right side: electrospun and left: SB-spun.

sample. PLA fibers (Figure 2(a)) had the most consistent morphology with small variations in diameter for both solution blow spinning and electrospinning (Table 3). On the other hand, PCL fibers when spun by SBS (Figure 2(b)) showed a very irregular structure with variable-sized fibers in a network of beads. When using electrospinning, a more

regular structure was observed; that is, fibers had a more uniform cross-section. Nevertheless, numerous beads, which were much more irregular in size, were also present in electrospun samples. PEO fibers, like PLA, also had a regular morphology with small variations in diameter for both SBS and electrospinning (Figure 2(c)). Image analysis also

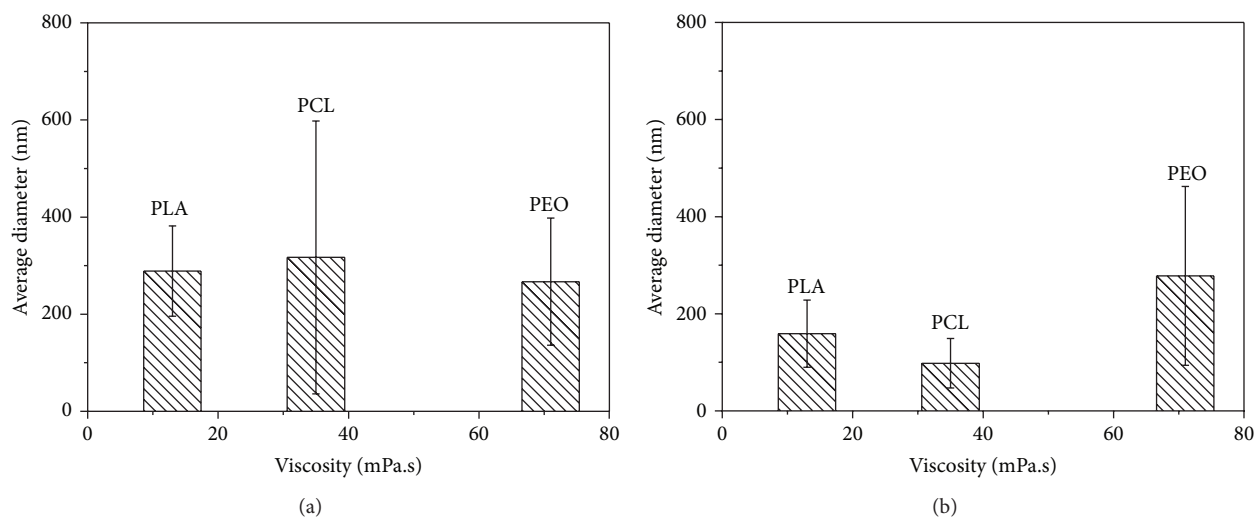


FIGURE 3: Effect of viscosity on fiber diameter and dispersion by (a) solution blow spinning and (b) electrospinning.

TABLE 3: Average diameter of spun fibers.

Polymer	(Average diameter \pm dispersion) (nm)	
	SB spun fibers	Electrospun fibers
PLA	289 \pm 93	159 \pm 69
PCL	317* \pm 281	98 \pm 51
PEO	267 \pm 131	278 \pm 184

*1% of the fibers observed has 3 μm of diameter.

showed that many of these fibers are broken, possibly due to their brittle nature.

A plot of fiber dispersion as a function of zero-shear viscosity (ZSV) of the polymers is shown in Figure 3, outlining an increase in fiber dispersion as zero-shear viscosity increases. It can be observed that higher ZSV values led to a greater dispersion for solution blow spun fibers. This might have happened because the air pressure exiting the outer nozzle was not high enough to stretch the fibers being produced. As viscosity increases, fiber stretching becomes more difficult, and as a consequence, thick fibers are potentially produced with broader fiber diameter distribution. One likely explanation is that a balance must be achieved between solution viscosity and the fiber-forming forces that are derived from the pressurized air exiting the outer nozzle in order to produce fibers with regular cross-sections.

During fiber formation by SBS, a jet of polymer solution is subjected to aerodynamic drag [26–28]. The shear forces that act upon the polymer solutions are therefore responsible for fiber stretching and, ultimately, for fiber diameter distribution [27]. One can speculate that higher air turbulence due to high air flow would lead to a larger distribution of fiber diameter because of the irregular air flow exiting the nozzle. Variations in air flow would then impart different degrees of stretching and shearing on fibers being formed. However, higher air flow was generally required because the viscosity of the polymer solution is high. For higher viscosity polymer solutions, fiber stretching would become more difficult, less

efficient, and unstable giving rise to broader fiber diameter distribution. Accordingly, the PLA system, with the lowest viscosity, produces the least variation in fiber diameter. Diameter histograms of spun fibers are shown in Figure 4.

In contrast, fiber formation in electrospinning is controlled by electrostatic repulsive forces that overcame surface tension, while a charged jet is ejected through a needle to produce fibers. As this jet travels through the air, the solvent evaporates, leaving behind ultrafine polymer fibers. Stretching by electric forces taking place on the surface of the jet is an important step during fibers formation [7]. Therefore, in electrospinning, fiber formation is more dependent on surface tension as can be seen by comparing average fiber diameter in Table 3 with surface tension in Table 2.

3.3. FTIR Characterization. FTIR spectra of spun fibers of PLA, PCL, and PEO solution blow spun fibers were recorded in the 600–3,000 cm^{-1} region. Similar spectra were obtained for electrospun fibers. Peak assignments for these polymers can be found in Figure 5 and Table 4.

3.3.1. PLA. In the PLA spectrum, the active modes overlapped to give a broad asymmetric band at about 1754 cm^{-1} . It is clear that C=O stretching mode is sensitive to morphology and chain conformation. According to Kister et al. [29], the intensity of the shoulder at 1754 cm^{-1} increases with the degree of syndiotacticity of polymer. The band observed at 1754 cm^{-1} for amorphous compounds was considered as resulting from entrainment of particular chiral unit generated by the pair addition mechanism [29, 30].

The CH_3 asymmetric deformation modes appeared at about 1452 cm^{-1} as an intense IR band (Table 4). Their stability in frequency reflected a pure vibrational mode. This region was characterized by a band at 1360 cm^{-1} . The 1182 cm^{-1} band observed in PLA could be assigned to a symmetric C–O–C stretching mode of ester groups. Asymmetric C–O–C modes were observed at 1086 cm^{-1} as a nonsymmetric IR

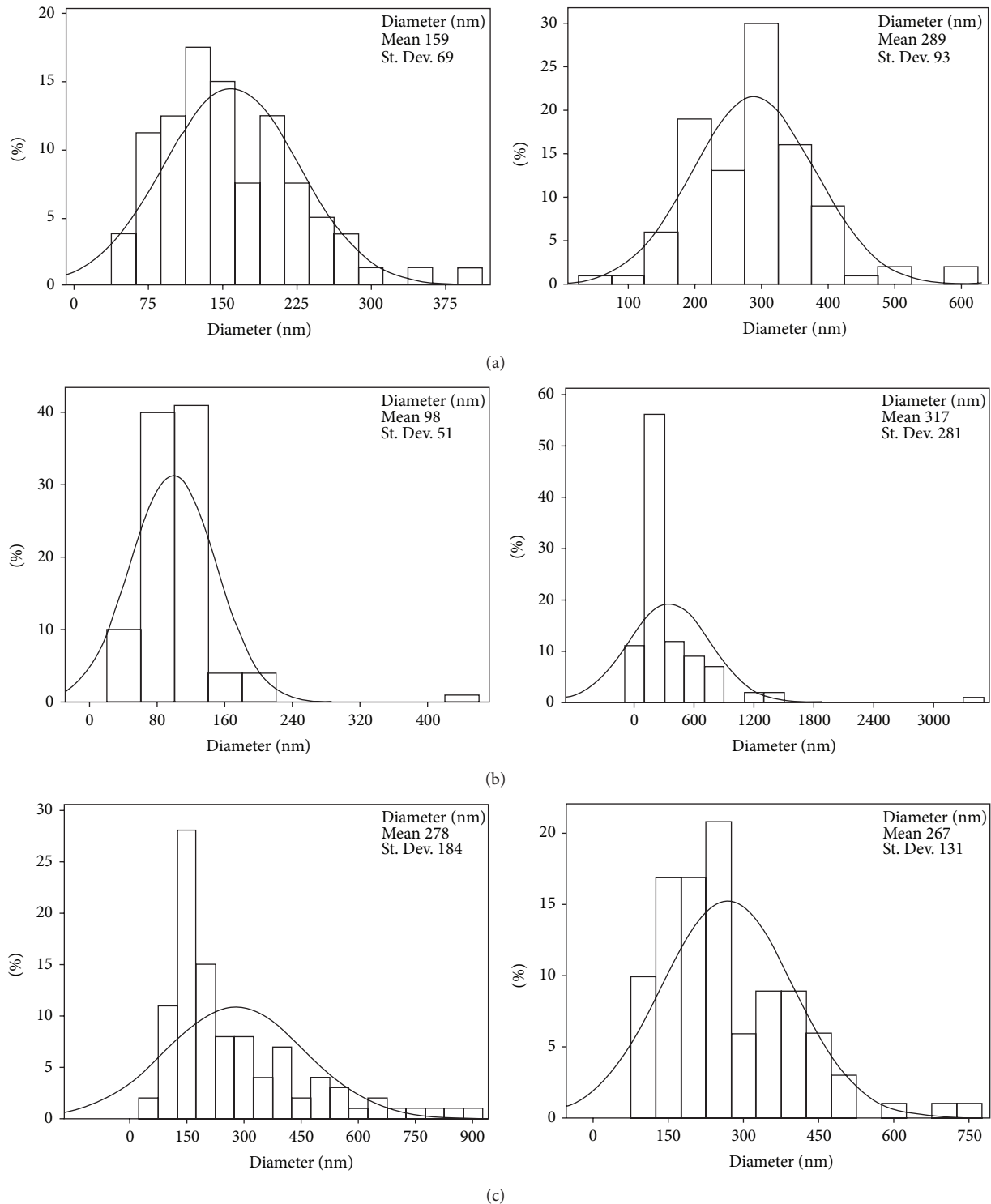


FIGURE 4: Diameter histograms of spun fibers obtained by solution blow spinning and electrospinning for PLA (a), PCL (b), and PEO (c). Right side: electrospun and left: SB-spun.

band. Other bands were assigned as follows: the band near 1045 cm^{-1} corresponded to $\nu\text{C}-\text{CH}_3$ stretching and the band 868 cm^{-1} to $\nu\text{C}-\text{COO}$ stretching.

3.3.2. PEO. The infrared spectra of PEO spun fibers were recorded, and the observed wavenumbers are listed in

Table 4. The spectrum is essentially the same as the spectrum of the crystalline PEO reported previously [31–33].

The strong band observed at 1110 cm^{-1} was assigned to the skeletal stretching mode. This assignment is confirmed by Miyazawa et al. [32] who associated this band with the C–O–C asymmetric stretching mode. The doublet at 963 and

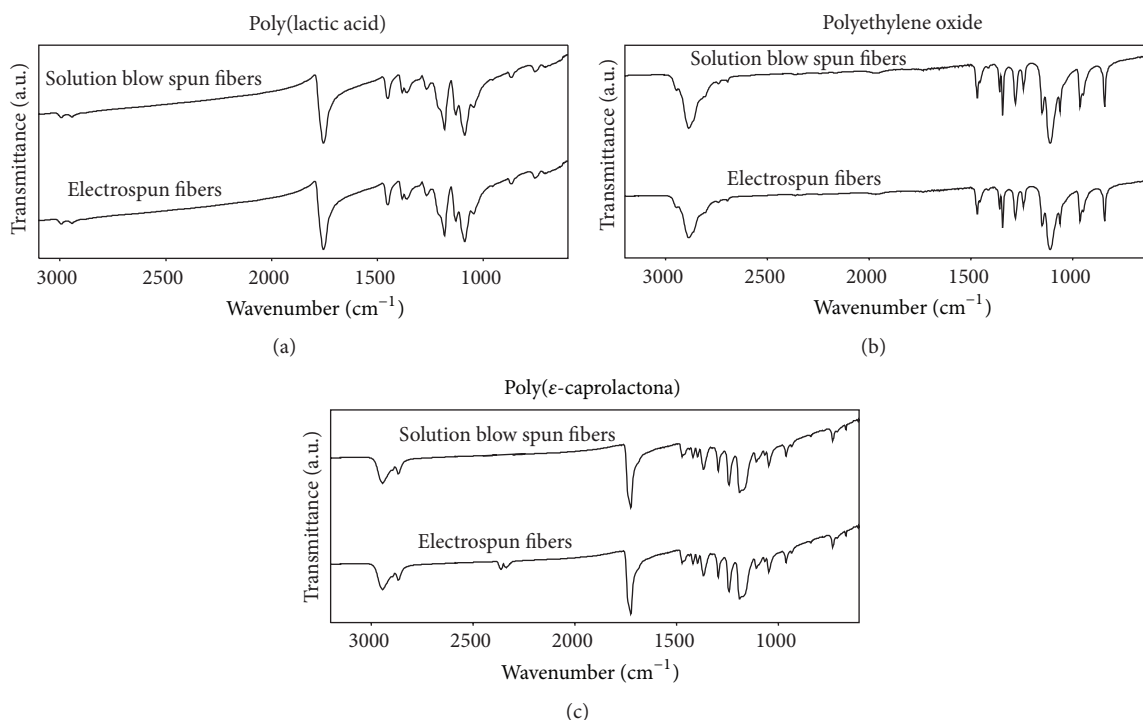


FIGURE 5: FTIR spectra for (a) PLA, (b) PEO, and (c) PCL.

947 cm^{-1} has been much discussed in parallel with the conformation of the CH_2 groups. This band had been assigned to the symmetric CH_2 rocking mode of the $\text{O}-\text{CH}_2\text{CH}_2-\text{O}$ group in the gauche conformation [33, 34] although Miyazawa et al. [32] assigned this band to the asymmetric rocking mode. The weak band at 947 cm^{-1} is due to the hybridized mode of the $\text{C}-\text{O}-\text{C}$ asymmetric stretching and the CH_2 symmetric rocking mode. Three strong bands are observed at 1148 , 1062 , and 843 cm^{-1} . The band at 843 cm^{-1} has been assigned previously to the CH_2 asymmetric rocking mode of the CH_2 group in the gauche conformation. The band at 1148 cm^{-1} is primarily due to the CH_2 symmetric rocking mode, whereas the band at 1062 cm^{-1} is primarily due to the $\text{C}-\text{O}-\text{C}$ asymmetric stretching mode coupled with the CH_2 symmetric rocking mode.

3.3.3. PCL. Regarding the PCL spectrum, strong bands such as the carbonyl stretching mode around 1726 cm^{-1} can be easily identified. Such as PLA and PEO, the important band and their assignments are outlined in Table 4. It is important to mention that some of these bands are only observed after band deconvolution, which is the case in the $1100\text{--}1190\text{ cm}^{-1}$ region, where three bands could be distinguished on the spectrum, while indeed three bands are overlapping. According to Coleman and Zarian [35], the band at 1294 cm^{-1} is assigned to the backbone $\text{C}-\text{C}$ and $\text{C}-\text{O}$ stretching modes in the crystalline PCL (see Table 4). He and Inoue [36] established a procedure for the quantitative crystallinity for analysis of PCL using a deconvolution of carbonyl vibration region (1726 cm^{-1}) into two bands (amorphous and crystalline).

In summary, close inspection of the spectra above revealed the absence of peaks that are characteristics of the solvents used for fiber spinning, therefore indicating that there are no residual solvents left after spinning. This is an important factor in applications such as in scaffolds for cell and tissue growth since solvent residue may be harmful in biomedical applications.

3.4. XRD Characterization. In order to determine the crystal structures in spun polymer fibers, X-ray diffraction was carried out. A comparison in terms of crystallinity, d -spacing and crystallite size (D) were also carried out and are summarized in Figure 6 and Table 5.

3.4.1. PLA. Comparative studies for PLA cast films and electrospun fibers are reported in the literature [37]. It is observed that nonwoven PLA spun fibers (Table 5) showed a strong amorphous halo, with one crystal peak found in the diffraction patterns (16.38°). On the other hand, solution blow spun and electrospun PLA fibers clearly exhibited two reflection peaks (near 13° and 16°), ascribed to α crystals, and a small peak (near 24°) associated with β phase [38, 39]. Formation of β crystals is caused by the different extent of deformation of the polymer molecules during fiber formation by solution blow spinning compared to electrospinning [39]. The critical factor for crystal formation is a high degree of deformation (present in both spinning processes) which was not observed for cast films. It can also be noted that α crystal peaks of electrospun fibers from PLA shifted toward higher 2θ values and larger crystallites were also present when compared with solution blow spun fibers and cast films.

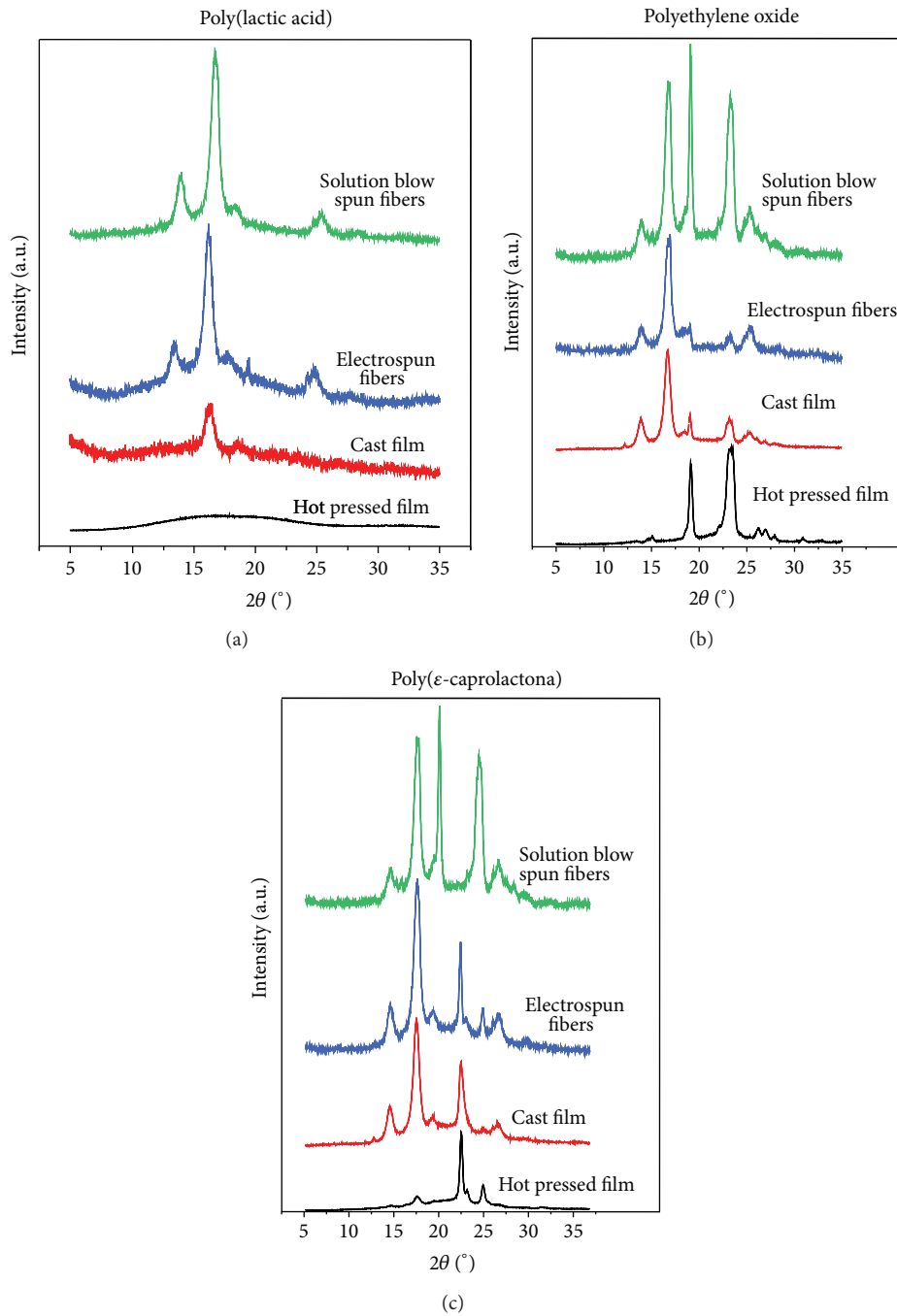


FIGURE 6: XRD patterns for (a) PLA, (b) PEO, and (c) PCL.

This fact is probably due to a different degree of stretching during crystallization, resulting in crystallites with variations in relative defects. Decreased order would appear as peak broadening and a greater variation in unit cell parameters from “ideal” crystals. PLA cast films presented a crystallinity of 35%, based in the Lorentz fit, while electrospun and solution blow spun fibers presented crystallinity, respectively, of 82 and 71% (Table 5). This increase in crystallinity observed for PLA spun fibers, when compared with PLA cast films, is attributed to the high stretching of the polymer chains which lead to a higher degree of molecular organization.

3.4.2. PEO. X-ray diffraction (XRD) patterns of PEO cast films and spun fibers were carried out, and the results are summarized in Table 5. PEO is a semicrystalline polymer with diffraction peaks at $2\theta = 19$ and 23° [33]. Distinct peaks characteristic of PEO crystallites ($2\theta = 14, 17,$ and 25°) were observed for spun fibers which indicate that solvent-induced polymer crystallization occurred.

When comparing SBS and electrospun fibers with cast films, it is interesting to note that SBS increased crystallinity, while electrospinning decreased relative crystallinity (Table 5). As a consequence, crystals developed under SBS

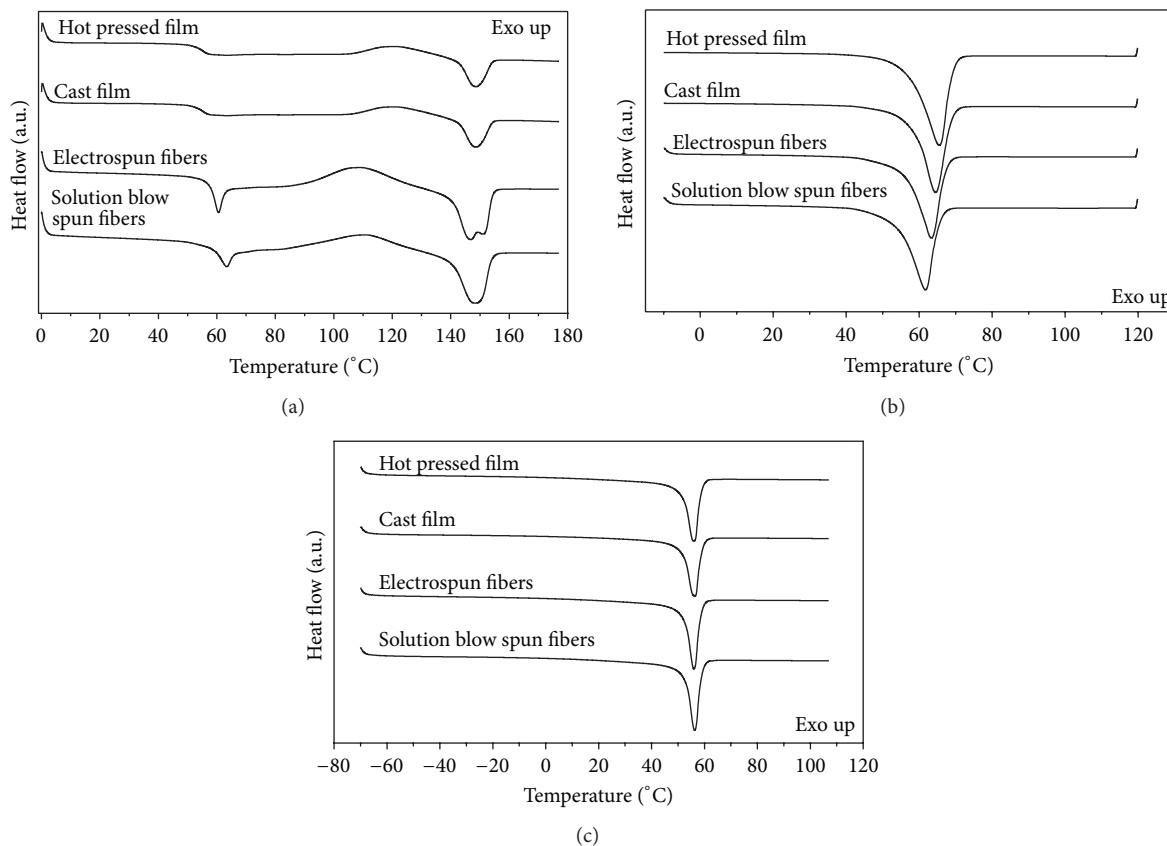


FIGURE 7: DSC curves for (a) PLA, (b) PEO, and (c) PCL.

were larger than those under electrospinning (Table 5). This fact suggests that in the crystallization of the fibers produced by electrospinning, the nucleation step is predominant, whereas in SBS the crystallite growth step is more predominant. Another factor that may have contributed to this difference, besides the nature of the forces involved, can be the timescale for each event to take place. SBS is depositing a much greater amount of polymer than electrospinning; it is roughly 10 times faster. The higher speed and greater forces in SBS likely favored chain orientation, leading to a higher crystallinity relative to electrospinning.

3.4.3. PCL. XRD patterns of PCL spun mats show that all diffraction peaks correspond to PCL, which is a semicrystalline polymer with two distinct diffraction peaks reported at ~ 21 and $\sim 23^\circ$ [40]. Moreover, these peaks were sharp and distinct, which indicated that samples were highly crystalline. Table 5 shows the degree of crystallinity, d -spacing, and crystallite size obtained from XRD for all samples. Crystallinity measurements for PCL range between 56 and 81%. Crystallite size and interplanar distance range between 1.7–3.9 nm and 4.6–5.3 nm, respectively. Similar to the behavior for PEO, electrospinning also reduced fiber crystallinity relative to cast films, while SBS increased fiber crystallinity. This also led to larger crystals when the morphology was developed under SBS, as opposed to electrospinning. Again, this clearly indicates that fiber formation mechanism in SBS is different

from electrospinning, and probably, a different timescale also governs the SBS process.

In summary, similar to electrospinning, the crystalline structure of polymer nanofibers obtained by solution blow spinning depends on process variables such as molecular weight, polymer-solvent interactions, and dynamics of fiber formation.

3.5. Thermal Analyses. TG and DSC results of spun fibers and films can be found in Table 6 and Figure 5. Characteristic temperatures (glass, crystallization, and melting), heat of fusion (ΔH_f), and crystallization (ΔH_c) for PLA, PEO, and PCL films obtained by casting, SB-spinning, and electrospinning are summarized in Table 6.

3.5.1. PLA. TG curves of PLA show that PLA cast films and spun nanofibers decomposed in a single step (Table 6). However, the onset of the decomposition temperature for PLA nanofibers was 327 and 311°C, respectively, for electrospun and SBS fibers, while for PLA cast films it was 333°C. A slight decrease in thermal stability for spun fibers, as opposed to cast films, is observed by TG, which might be due to their high surface area (Table 6). A very similar thermal behavior has already been reported in the literature [41, 42]. It must be noted that the surface areas of spun nanofibers are much higher than those of cast films.

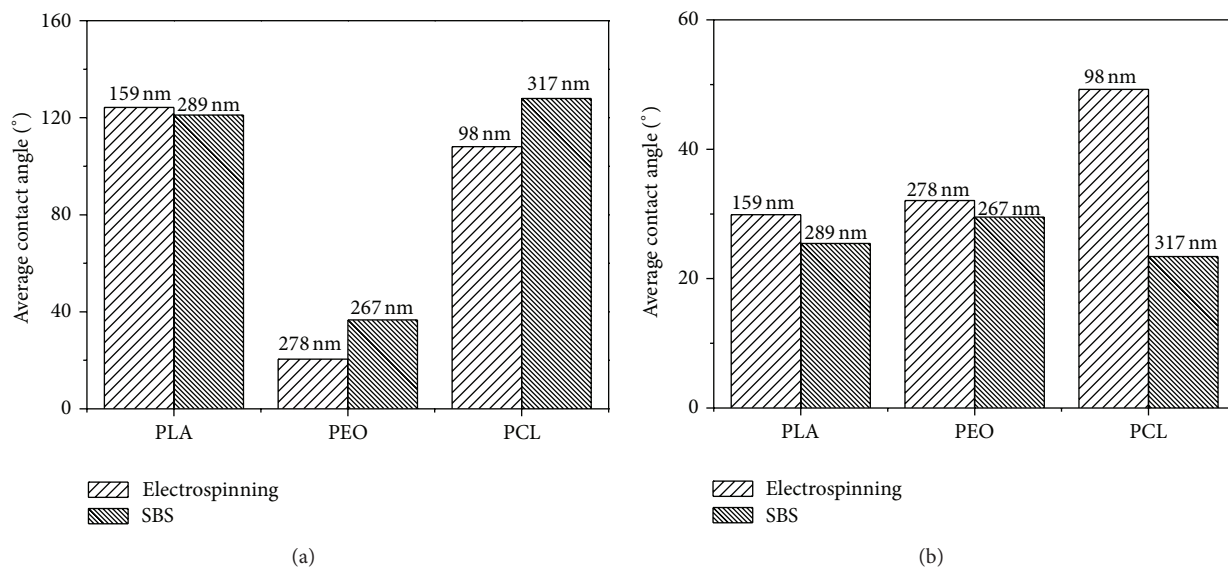


FIGURE 8: Effect of the fiber average diameters on contact angle (a) water and (b) ethylene glycol as a function of the spinning technique.

TABLE 4: Characteristic infrared bands of PLA, PEO, and PCL.

Polymer	Position (cm ⁻¹)	Vibrational mode	Abbreviation
PLA	2993	Asymmetrical stretching	$\nu_{as}(CH_2)$
	2943	Symmetrical stretching	$\nu_s(CH_2)$
	1755	Stretching	$\nu(C=O)$
	1450	Asymmetrical scissoring	$\delta_{as}(CH_3)$
	1360	Symmetrical scissoring	$\delta_s(CH_3)$
	1182	Asymmetrical stretching + twisting	$\nu_{as}(C-O) + \tau(CH_3)$
	1086	Symmetrical stretching	$\nu_s(C-O-C)$
	1045	Symmetrical stretching	$\nu_s(C-CH_3)$
	868	Stretching	$\nu(C-COO)$
PEO	2946	Asymmetrical stretching	$\nu_{as}(CH_2)$
	2886	Symmetrical stretching	$\nu_s(CH_2)$
	1468	Scissoring	$\delta(CH_2)$
	1361	Wagging	$\omega(CH_2)$
	1343	Wagging	$\omega(CH_2)$
	1281	Twisting	$\tau(CH_2)$
	1242	Twisting	$\tau(CH_2)$
	1150	Stretching	$\nu(CO)$
	1110	Stretching	$\nu(CO)$
	1062	Stretching	$\nu(CO)$
	963	Rocking	$\rho(CH_2)$
843	Rocking	$\rho(CH_2)$	
PCL	2946	Asymmetrical stretching	$\nu_{as}(CH_2)$
	2864	Symmetrical stretching	$\nu_s(CH_2)$
	1726	Stretching	$\nu(C=O)$
	1294	Stretching	$\nu_{crystalline}$
	1243	Asymmetrical stretching	$\nu_{as}(C-O-C)$
	1192	Stretching	$\nu(OC-O)$
	1180	Symmetrical stretching	$\nu_s(C-O-C)$
	1162	Stretching	$\nu_{amorphous}$

TABLE 5: Crystalline structure parameters for PLA, PEO, and PCL.

Polymer	Crystallinity (%)	d -spacing (\AA)	D (\AA)	R^2 (Lorentz model)
PLA _C *	35	5.4	1.4	0.96
PLA _{ES}	82	5.3	1.7	0.97
PLA _{SBS}	71	5.4	1.4	0.91
PEO _C	74	5.3	1.9	0.98
PEO _{ES}	57	5.3	2.0	0.97
PEO _{SBS}	93	4.6	4.1	0.97
PCL _C	56	5.3	2.0	0.99
PCL _{ES}	75	5.3	1.7	0.98
PCL _{SBS}	81	4.6	3.9	0.98

*C: cast; ES: electrospinning; SBS: solution blow spinning.

TABLE 6: Characteristic temperatures and heat of fusion (ΔH_f) and crystallization (ΔH_c) for PLA, PEO, and PCL films obtained by casting, SB-spinning, and electrospinning.

Polymer	T_g ($^{\circ}$)	T_c ($^{\circ}$)	T_m ($^{\circ}$)	T_d ($^{\circ}$)	ΔH_f (J/g)	ΔH_c (J/g)
PLA _C *	60	108	147	333	17	5
PLA _{ES}	61	109	147	327	30	24
PLA _{SBS}	59	112	150	311	23	15
PEO _C	—	43	65	373	103	0
PEO _{ES}	—	46	63	375	110	0
PEO _{SBS}	—	44	62	371	146	0
PCL _C	—	19	57	380	29	0
PCL _{ES}	—	28	56	380	29	0
PCL _{SBS}	—	29	56	379	38	0

*C: cast; ES: electrospinning; SBS: solution blow spinning.

As is well noted in the literature [12], crystalline PLA fibers can exhibit two distinct crystalline morphologies, the α structure, with lamellar-folded chain morphology, and metastable β structure, with a planar “zigzag,” extended chain morphology. These are noted by two distinct peaks near the melting point. Figure 7(a) shows DSC curves for electrospun and solution blow spun PLA fibers with different average diameters compared with PLA cast films.

The lower cold crystallization temperature of electrospun fibers compared to SBS fibers (Table 6) suggested that electrospun fibers had a certain level of chain alignment that led to crystallization occurring at a lower temperature. Zong et al. [43] investigated PLA nanofibers with DSC and XRD analysis and found that polymer chains were noncrystalline but highly oriented.

3.5.2. *PEO*. Typical weight loss (TG) and derivative (DTG) curves (inset plots) of spun and cast films of PEO were obtained, and the results are presented in Table 6. The onset of the decomposition curves of these polymers is summarized in Table 6. The onset decomposition temperature of PEO cast films was 373°C and for spun fiber was found to be 375 and 371°C , respectively, for electrospun and SBS. PEO cast films show a thermal stability similar to that of spun fibers. TG

curves of both spun fibers and cast film also indicate one reaction step (Table 6). This behavior is somewhat unexpected since both fibers produced by electrospinning and SBS have very high surface area when compared to films which can be due to the higher degree of crystallinity developed during fiber formation.

DSC analysis of PEO in hot pressed form presented a melting temperature (T_m) of 62°C ($\Delta H_f = 109$ J/g), whereas cast film and electrospun PEO nanofibers were determined at 65°C ($\Delta H_f = 103$ J/g) and 63°C ($\Delta H_f = 110$ J/g), respectively, during the first heating cycle (Figure 7(b); Table 6). In addition, the PEO fibers produced by solution blow spinning presented a melting temperature of 62°C ($\Delta H_f = 143$ J/g) in the first heating cycle, indicating an increase in crystallinity of fibers by solution blow spinning process.

3.5.3. *PCL*. The TG curve obtained for spun and cast films of PCL displays one main degradation step with an inflection point at 380°C for PCL cast films and spun fibers. The DSC curves of the PCL fiber mats and hot pressed and cast film forms are shown in Figure 7(c). It can be seen from the first heating run (Figure 7(c) and Table 6) that in all cases the melting point (T_m) of PCL was 56°C . Their fusion enthalpies were 32 J/g for hot pressed form, 29 J/g for cast film and electrospun forms and 38 J/g for solution blow spun form. Such as PEO case, these results indicate that there was little to no variation in T_m with the processing method.

The crystalline structure developed in PCL nanofibers by electrospinning, as well as molecular orientation, is different from as-received materials, as reported in the literature [6, 12, 40, 44]. In electrospinning and SBS processes, rapid solidification occurs due to quick solvent evaporation. Because of this, solvent properties and polymer-solvent interactions play important roles in polymer crystallinity and chain orientation of the spun fibers. Since molecular chains do not have enough time to form a fully crystalline structure, development of crystallinity under a fast solidification is impacted. This particularly affects flexible polymers with lower glass transition (T_g) temperatures, which have more mobility at their process temperatures and crystallize in a shorter time than a rigid polymer with high T_g .

T_g values for PLA, PEO, and PCL are, respectively, 60 , -11 , and -72°C . Consequently, PEO and PCL crystallization

can be facilitated by chain stretching during fiber formation under SBS and electrospinning, even after PEO and PCL are solidified. These may be the reasons why solution blow spun fibers of PEO and PCL developed higher crystallinity, whereas the crystallization of PLA was reduced. Moreover, the DL structure of PLA is another factor that is, responsible for its crystallinity. Polymerization of a racemic mixture of L- and D-lactides forms poly-D,L-lactide (PLA), which is amorphous and has a glass transition temperature of 55–60°C. The degree of crystallinity can be tuned by altering the ratio of D to L enantiomers within the polymer. Selection of the PLA stereochemistry can have a major effect on the polymer properties, processability, and biodegradability [45]. These results of thermal analysis and X-ray diffraction suggest that the fast solvent evaporation occurs by different mechanisms in SBS and electrospinning. This can be related to the atmosphere surrounding these processes. In the latter case, it is predominantly controlled by the characteristics (relative humidity type of gas, temperature, etc.) of the pressurized gas.

3.6. Contact Angle Measurements. For determination of the hydrophilic character of the spun nonwoven nanofibers, the contact angle between the mats and the water and ethylene glycol was measured. It is known that the lower the contact angle, the higher the hydrophilic nature of the surface. Changes of the contact angle values between the water/ethylene glycol with the different spun fibers (PLA, PCL, and PEO) are illustrated in Figure 8.

It is reported in the literature [46–48] that polyesters and polyethers are not highly hydrophobic materials (PLA, PCL, and PEO cast film shows a contact angle of 84°, 89°, and 48°, resp.); the initial hydrophobicity of the as-spun mats is metastable; that is, contact angle decreases gradually with time over a period of about 2 min under ambient conditions. Ma et al. [49] attributed the origin of this decrease in contact angle from the evaporation of water from the droplet and the conversion of the contact zone from an initial Cassie-Baxter state to a final Wenzel state as the water droplet sinks into the pores of the mat due to capillarity. The changes in contact angle as a function of the average fiber diameter for water droplets (dipole moment 1.84 D) and ethylene glycol (dipole moment 2.31 D) can be observed in Figure 8.

A parabolic behavior was observed for both electrospun and solution blow spun fibers. It is believed that these variations in contact angle are associated with the average fiber diameter. Moreover, the porous nature of spun mats acts as roughness in the nanoscale. It is well known that if a polymer is hydrophobic, increasing its roughness causes an increase in the hydrophobicity of this polymer; on the other hand, if the polymer is hydrophilic, its hydrophilicity is also found to increase with increasing surface roughness.

As a general summary, solution blow spinning and electrospinning of polymers from solution may yield submicron and nanometric fibers which are characterized by several structures (fiber, bead, and network), depending on the working conditions used. Fibers formation is apparently controlled by a rapid evaporation of the solvent and a high

strain rate caused by electrical forces (electrospinning) and aerodynamic forces (SBS). The fibers obtained by solution blow spinning have properties which make them ideal candidates for cell adhesion, catalysis, and sensors applications.

4. Conclusions

Electrospinning and solution blow spinning of PLA, PEO and PCL from solution yield fibers whose diameters range from the nanometer to the submicron scale. Polymer molecular weight, surface tension, and evaporation rate of polymer solutions contribute to fiber diameter. These fibers can possess different morphologies, such as fibers with and without beads, and fiber bundles which can be controlled by process variables. In both techniques, morphology development is apparently controlled by solvent evaporation and a subsequent rapid solidification. Nonwoven mats are of interest for a broad range of applications in areas such as tissue engineering or drug delivery given the absence of residual solvents in the SBS fibers for PLA, PCL and PEO, which was confirmed by FTIR studies. XRD analysis indicated that either a different mechanism or a timescale, or both, may be playing an important role in fiber crystallinity development by electrospinning and SBS. Therefore, crystalline structure and chain orientation in polymer nanofibers electrospun and solution blow spun depend on process variables such as molecular weight, polymer-solvent interactions, and process timescale. PLA nanofibers presented a decreased thermal stability compared to powder PLA, but this effect was not observed for PEO and PCL. In addition, DSC analysis showed two peaks near the melting point (α and β crystalline phases) for PLA spun samples. Thermal analysis showed that PEO and PCL crystallization can be facilitated by chain stretching during fiber formation by SBS and electrospinning, even after PEO and PCL are solidified. These may be the reasons why solution blow spun fibers of PEO and PCL developed higher crystallinity, whereas the crystallization of PLA was reduced.

Acknowledgments

The authors acknowledge the financial support provided by the Brazilian Ministry of Science and Technology (MCT/FINEP) and the National Research Councils (CAPES and CNPQ). The authors are grateful to the Bernhard Gross Polymer Group (IFSC/USP) for their assistance with surface tension measurements.

References

- [1] M. Bognitzki, W. Czado, T. Frese et al., “Nanostructured fibers via electrospinning,” *Advanced Materials*, vol. 13, no. 1, p. 70, 2001.
- [2] C. J. Ellison, A. Phatak, D. W. Giles, C. W. Macosko, and F. S. Bates, “Melt blown nanofibers: fiber diameter distributions and onset of fiber breakup,” *Polymer*, vol. 48, no. 11, pp. 3306–3316, 2007.
- [3] R. S. Rao and R. L. Shambaugh, “Vibration and stability in the melt blowing process,” *Industrial & Engineering Chemistry Research*, vol. 32, no. 12, pp. 3100–3111, 1993.

- [4] R. L. Shambaugh, "A macroscopic view of the melt-blowing process for producing microfibers," *Industrial & Engineering Chemistry Research*, vol. 27, no. 12, pp. 2363–2372, 1988.
- [5] P. J. Barham and A. Keller, "High-strength polyethylene fibres from solution and gel spinning," *Journal of Materials Science*, vol. 20, no. 7, pp. 2281–2302, 1985.
- [6] J. M. Deitzel, J. Kleinmeyer, D. Harris, and N. C. Beck Tan, "The effect of processing variables on the morphology of electrospun nanofibers and textiles," *Polymer*, vol. 42, no. 1, pp. 261–272, 2001.
- [7] J. Doshi and D. H. Reneker, "Electrospinning process and applications of electrospun fibers," *Journal of Electrostatics*, vol. 35, no. 2-3, pp. 151–160, 1995.
- [8] Z. M. Huang, Y. Z. Zhang, M. Kotaki, and S. Ramakrishna, "A review on polymer nanofibers by electrospinning and their applications in nanocomposites," *Composites Science and Technology*, vol. 63, no. 15, pp. 2223–2253, 2003.
- [9] S. A. Theron, E. Zussman, and A. L. Yarin, "Experimental investigation of the governing parameters in the electrospinning of polymer solutions," *Polymer*, vol. 45, no. 6, pp. 2017–2030, 2004.
- [10] M. C. Branciforti, T. A. Custodio, L. M. Guerrini, L. Averous, and R. E. S. Bretas, "Characterization of nano-structured poly(D,L-lactic acid) nonwoven mats obtained from different solutions by electrospinning," *Journal of Macromolecular Science B*, vol. 48, no. 6, pp. 1222–1240, 2009.
- [11] W. K. Son, J. H. Youk, T. S. Lee, and W. H. Park, "The effects of solution properties and polyelectrolyte on electrospinning of ultrafine poly(ethylene oxide) fibers," *Polymer*, vol. 45, no. 9, pp. 2959–2966, 2004.
- [12] J. Zeng, X. S. Chen, Q. Z. Liang, X. L. Xu, and X. B. Jing, "Enzymatic degradation of poly(L-lactide) and poly(epsilon-caprolactone) electrospun fibers," *Macromolecular Bioscience*, vol. 4, no. 12, pp. 1118–1125, 2004.
- [13] Q. P. Pham, U. Sharma, and A. G. Mikos, "Electrospinning of polymeric nanofibers for tissue engineering applications: a review," *Tissue Engineering*, vol. 12, no. 5, pp. 1197–1211, 2006.
- [14] E. S. Medeiros, G. M. Glenn, A. P. Klamczynski, W. J. Orts, and L. H. C. Mattoso, "Solution blow spinning: a new method to produce micro- and nanofibers from polymer solutions," *Journal of Applied Polymer Science*, vol. 113, no. 4, pp. 2322–2330, 2009.
- [15] J. E. Oliveira, V. Zucolotto, L. H. C. Mattoso, and E. S. Medeiros, "Multi-walled carbon nanotubes and poly(lactic acid) nanocomposite fibrous membranes prepared by solution blow spinning," *Journal of Nanoscience and Nanotechnology*, vol. 1, no. 1, 2011.
- [16] S. Sinha-Ray, A. L. Yarin, and B. Pourdeyhimi, "The production of 100/400 nm inner/outer diameter carbon tubes by solution blowing and carbonization of core-shell nanofibers," *Carbon*, vol. 48, no. 12, pp. 3575–3578, 2010.
- [17] J. E. Oliveira, E. A. Moraes, R. G. F. Costa et al., "Nano and submicrometric fibers of poly(D,L-lactide) obtained by solution blow spinning: process and solution variables," *Journal of Applied Polymer Science*, vol. 122, no. 5, pp. 3396–3405, 2011.
- [18] E. S. Medeiros, G. M. Glenn, A. P. Klamczynski, W. J. Orts, and L. H. C. Mattoso, "Solution blow spinning: a new method to produce micro- and nanofibers from polymer solutions," *Journal of Applied Polymer Science*, vol. 113, no. 4, pp. 2322–2330, 2009.
- [19] D. W. Choi, K. G. Marra, and P. N. Kumta, "Chemical synthesis of hydroxyapatite/poly(epsilon-caprolactone) composites," *Materials Research Bulletin*, vol. 39, no. 3, pp. 417–432, 2004.
- [20] P. Huang, J. X. Zheng, S. W. Leng et al., "Poly(ethylene oxide) crystal orientation changes in an inverse hexagonal cylindrical phase morphology constructed by a poly(ethylene oxide)-block-polystyrene diblock copolymer," *Macromolecules*, vol. 40, no. 3, pp. 526–534, 2007.
- [21] M. Khayet and M. C. Garcia-Payo, "X-Ray diffraction study of polyethersulfone polymer, flat-sheet and hollow fibers prepared from the same under different gas-gaps," *Desalination*, vol. 245, no. 1–3, pp. 494–500, 2009.
- [22] C. Marega, A. Marigo, V. Dinoto, R. Zannetti, A. Martorana, and G. Paganetto, "Structure and crystallization kinetics of poly(L-Lactic Acid)," *Makromolekulare Chemie-Macromolecular Chemistry and Physics*, vol. 193, no. 7, pp. 1599–1606, 1992.
- [23] S. L. Shenoy, W. D. Bates, H. L. Frisch, and G. E. Wnek, "Role of chain entanglements on fiber formation during electrospinning of polymer solutions: good solvent, non-specific polymer-polymer interaction limit," *Polymer*, vol. 46, no. 10, pp. 3372–3384, 2005.
- [24] J. H. Yu, S. V. Fridrikh, and G. C. Rutledge, "The role of elasticity in the formation of electrospun fibers," *Polymer*, vol. 47, no. 13, pp. 4789–4797, 2006.
- [25] C. Pattamaprom, W. Hongrojjanawiwat, P. Koombhongse, P. Supaphol, T. Jarusuwanpoo, and R. Rangkupan, "The influence of solvent properties and functionality on the electrospinnability of polystyrene nanofibers," *Macromolecular Materials and Engineering*, vol. 291, no. 7, pp. 840–847, 2006.
- [26] S. Sinha-Ray, A. L. Yarin, and B. Pourdeyhimi, "Meltblowing: I-basic physical mechanisms and threadline model," *Journal of Applied Physics*, vol. 108, no. 3, Article ID 034912, 12 pages, 2010.
- [27] A. L. Yarin, S. Sinha-Ray, and B. Pourdeyhimi, "Meltblowing: multiple polymer jets and fiber-size distribution and lay-down patterns," *Polymer*, vol. 52, no. 13, pp. 2929–2938, 2011.
- [28] A. L. Yarin, S. Sinha-Ray, and B. Pourdeyhimi, "Meltblowing: II-linear and nonlinear waves on viscoelastic polymer jets," *Journal of Applied Physics*, vol. 108, no. 3, Article ID 034913, 10 pages, 2010.
- [29] G. Kister, G. Cassanas, and M. Vert, "Effects of morphology, conformation and configuration on the IR and Raman spectra of various poly(lactic acid)s," *Polymer*, vol. 39, no. 2, pp. 267–273, 1998.
- [30] J. Zhang, H. Tsuji, I. Noda, and Y. Ozaki, "Structural changes and crystallization dynamics of poly(L-lactide) during the cold-crystallization process investigated by infrared and two-dimensional infrared correlation spectroscopy," *Macromolecules*, vol. 37, no. 17, pp. 6433–6439, 2004.
- [31] A. C. Angood and J. L. Koenig, "Infrared studies of chain folding in polyethylene oxide," *Journal of Applied Physics*, vol. 39, no. 11, p. 4985, 1968.
- [32] T. Miyazawa, Y. Ideguchi, K. Fukushima et al., "Molecular vibrations and structure of high polymers .3. Polarized infrared spectra, normal vibrations, and helical conformation of polyethylene glycol," *Journal of Chemical Physics*, vol. 37, no. 12, p. 2764, 1962.
- [33] W. H. T. Davison, "Infrared spectra and crystallinity.3. Poly(Ethylene Glycol)," *Journal of the Chemical Society*, p. 3270, 1955.
- [34] I. Rey, J. C. Lassègues, J. Grondin, and L. Servant, "Infrared and Raman study of the PEO-LiTFSI polymer electrolyte," *Electrochimica Acta*, vol. 43, no. 10-11, pp. 1505–1510, 1998.

- [35] M. M. Coleman and J. Zarian, "Fourier-transform infrared studies of polymer blends-2. Poly(Epsilon-Caprolactone)-Poly(Vinyl Chloride) system," *Journal of Polymer Science Polymer Physics Edition*, vol. 17, no. 5, pp. 837–850, 1979.
- [36] Y. He and Y. Inoue, "Novel FTIR method for determining the crystallinity of poly(ϵ -caprolactone)," *Polymer International*, vol. 49, no. 6, pp. 623–626, 2000.
- [37] J. Ren, W. Liu, J. Zhu, and S. Gu, "Preparation and characterization of electrospun, biodegradable membranes," *Journal of Applied Polymer Science*, vol. 109, no. 5, pp. 3390–3397, 2008.
- [38] W. Hoogsteen, A. R. Postema, A. J. Pennings, G. Ten Brinke, and P. Zugenmaier, "Crystal structure, conformation, and morphology of solution-spun poly(L-lactide) fibers," *Macromolecules*, vol. 23, no. 2, pp. 634–642, 1990.
- [39] H. J. Zhou, T. B. Green, and Y. L. Joo, "The thermal effects on electrospinning of polylactic acid melts," *Polymer*, vol. 47, pp. 7497–7505, 2006.
- [40] K. H. Lee, H. Y. Kim, M. S. Khil, Y. M. Ra, and D. R. Lee, "Characterization of nano-structured poly(ϵ -caprolactone) nonwoven mats via electrospinning," *Polymer*, vol. 44, no. 4, pp. 1287–1294, 2003.
- [41] C. Carrizales, S. Pelfrey, R. Rincon et al., "Thermal and mechanical properties of electrospun PMMA, PVC, Nylon 6, and Nylon 6,6," *Polymers for Advanced Technologies*, vol. 19, no. 2, pp. 124–130, 2008.
- [42] J. S. Kim and D. S. Lee, "Thermal properties of electrospun polyesters," *Polymer Journal*, vol. 32, no. 7, pp. 616–618, 2000.
- [43] X. Zong, K. Kim, D. Fang, S. Ran, B. S. Hsiao, and B. Chu, "Structure and process relationship of electrospun bioabsorbable nanofiber membranes," *Polymer*, vol. 43, no. 16, pp. 4403–4412, 2002.
- [44] J. Zeng, X. Chen, X. Xu et al., "Ultrafine fibers electrospun from biodegradable polymers," *Journal of Applied Polymer Science*, vol. 89, no. 4, pp. 1085–1092, 2003.
- [45] K. A. Athanasiou, G. G. Niederauer, and C. M. Agrawal, "Sterilization, toxicity, biocompatibility and clinical applications of polylactic acid/polyglycolic acid copolymers," *Biomaterials*, vol. 17, no. 2, pp. 93–102, 1996.
- [46] F. Chen, C. N. Lee, and S. H. Teoh, "Nanofibrous modification on ultra-thin poly(epsilon-caprolactone) membrane via electrospinning," *Materials Science & Engineering C*, vol. 27, no. 2, pp. 325–332, 2007.
- [47] W. R. Gombotz, W. Guanghai, T. A. Horbett, and A. S. Hoffman, "Protein adsorption to poly(Ethylene Oxide) surfaces," *Journal of Biomedical Materials Research*, vol. 25, no. 12, pp. 1547–1562, 1991.
- [48] K. Kim, M. Yu, X. H. Zong et al., "Control of degradation rate and hydrophilicity in electrospun non-woven poly(D,L-lactide) nanofiber scaffolds for biomedical applications," *Biomaterials*, vol. 24, no. 27, pp. 4977–4985, 2003.
- [49] M. Ma, Y. Mao, M. Gupta, K. K. Gleason, and G. C. Rutledge, "Superhydrophobic fabrics produced by electrospinning and chemical vapor deposition," *Macromolecules*, vol. 38, no. 23, pp. 9742–9748, 2005.



Hindawi

Submit your manuscripts at
<http://www.hindawi.com>

